

On non-vanishing amplitude of Hanle electromagnetically induced absorption in Rb

M. M. Mijailović, J. Dimitrijević, A. J. Krmpot, Z. D. Grujić, B. M. Panić, D. Arsenović, D. V. Pantelić, B. M. Jelenković

Institute of Physics, University of Belgrade, 11080 Belgrade, Serbia

brana.jelenkovic@phy.bg.ac.yu

Abstract: Amplitude and linewidths of the Hanle EIA, obtained from transmission of the laser locked to closed $F_g \rightarrow F_e = F_g + 1$ transitions in ^{85}Rb and ^{87}Rb , have maximum values at few mW/cm^2 . Amplitude of the EIA reaches steady value different from zero for higher laser intensities, even for laser intensities of $40 \text{ mW}/\text{cm}^2$. Theoretical model of EIA, for the same atomic system as in the experiment, show that the laser intensity, at which maximum of amplitudes and widths occur, depends on the laser detuning. For smaller laser detuning of a few tens of MHz, EIA has a maximum and then vanishes at higher laser intensities. For larger laser detuning of the order of hundreds MHz (but still in the range of Doppler broadening) amplitude of the EIA has very broad maximum and remains above zero for intensities above $40 \text{ mW}/\text{cm}^2$. Such theoretical results indicate that Hanle absorption peak remains in the experimental results, regardless of the laser intensities, due to Doppler effect.

© 2007 Optical Society of America

OCIS codes: 020.1670 (Coherent optical effects); 270.1670 (Coherent optical effects)

References and links

1. A. M. Akulshin, S. Barreiro, and A. Lezama, "Electromagnetically induced absorption and transparency due to resonant two-field excitation of quasidegenerate levels in Rb vapor," *Phys. Rev. A* **57**, 2996 (1998).
2. E. Arimondo, "Coherent population trapping in laser spectroscopy," *Prog. Opt.* XXXV, 257 (1996).
3. F. Renzoni, W. Maichen, L. Windholz, and E. Arimondo, "Coherent population trapping with losses observed on the Hanle effect of the D1 sodium line," *Phys. Rev. A* **55**, 3710 (1997).
4. A. V. Taichenachev, A. M. Tumaikin, and V. I. Yudin, "Electromagnetically induced absorption in a four-state system," *Phys. Rev. A* **61**, 011802(R), (1999).
5. F. Renzoni, C. Zimmermann, P. Verkerk, and E. Arimondo, "Enhanced absorption Hanle effect on the $F_g=F - F_e=F+1$ closed transitions," *J. Opt. B: Quantum Semiclass. Opt.* **3**, S7 (2001).
6. H. Failache, P. Valente, G. Ban, V. Lorent, and A. Lezama, "Inhibition of electromagnetically induced absorption due to excited-state decoherence in Rb vapor," *Phys. Rev. A* **67**, 043810 (2003).
7. J. Dalibard and C. Cohen-Tannoudji, "Laser cooling below the Doppler limit by polarization gradients: simple theoretical model," *J. Opt. Soc. Am.* **B 6**, 2023 (1989).
8. A. Aspect, E. Arimondo, R. Kaiser, N. Vansteenkiste and C. Cohen-Tannoudji, "Laser cooling below the one-photon recoil energy by velocity selective coherent population trapping," *Phys. Rev. Lett.* **61**, 826 (1988).
9. M. Fleischhauer and M. D. Lukin, "Dark-State Polaritons in Electromagnetically Induced Transparency," *Phys. Rev. Lett.* **84**, 5094 (2000).
10. A. M. Akulshin, A. Lezama, A. I. Sidorov, R. J. Mclean, and P. Hannaford, "Storage of light in an atomic medium using electromagnetically induced absorption," *J. Phys. B: At. Mol. Opt. Phys.* **38**, L365 (2005).
11. Giovanni Moruzzi and Franco Strumia, "The Hanle effect and level crossing spectroscopy," Plenum Press 1991.
12. F. Renzoni, S. Cartaleva, G. Alzetta, and E. Arimondo, "Enhanced absorption Hanle effect in the configuration of crossed laser beam and magnetic field," *Phys. Rev. A* **63**, 065401, (2001).

13. Y. Dancheva, G. Alzetta, S. Cartaleva, M. Taslakov, and Ch. Andreeva, "Coherent effects on the Zeeman sublevels of hyperfine states in optical pumping of Rb by monomode diode laser," *Opt. Commun.* **178**, 103 (2000).
14. G. Alzetta, S. Cartaleva, Y. Dancheva, Ch. Andreeva, S. Gozzini, L. Botti, and A. Rossi, "Coherent effects on the Zeeman sublevels of hyperfine states at the D1 and D2 lines of Rb," *J. Opt. B: Quantum Semiclass. Opt.* **3**, 181 (2001).
15. E. Alipieva, S. Gateva, E. Taskova, and S. Cartaleva, "Narrow structure in the coherent population trapping resonance in rubidium," *Opt. Lett.* **28**, 1817 (2003).
16. J. Alnis, K. Blush, M. Auzinsh, S. Kennedy, N. Shafer-Ray, and E. Abraham, "The Hanle effect and level crossing spectroscopy in Rb vapour under strong laser excitation," *J. Phys. B: At. Mol. Opt. Phys.* **36**, 1161 (2003).
17. A. Lipsich, S. Barreiro, A. M. Akulshin, and A. Lezama, "Absorption spectra of driven degenerate two-level atomic systems," *Phys. Rev. A* **61**, 053803 (2000).
18. K. Kim, M. Kwon, H. D. Park, H. S. Moon, H. S. Rawat, K. An, and J. B. Kim, "Electromagnetically induced absorption spectra depending on intensities and detunings of the coupling field in Cs vapour," *J. Phys. B: At. Mol. Opt. Phys.* **34**, 4801 (2001).
19. H. S. Moon, S. K. Kim, K. Kim, C. H. Lee, and J. B. Kim, "Atomic coherence changes caused by optical pumping applied to electromagnetically induced absorption," *J. Phys. B: At. Mol. Opt. Phys.* **36**, 3721 (2003).
20. C. Goren, A. D. Wilson-Gordon, M. Rosenbluh, and H. Friedmann, "Switching from positive to negative dispersion in transparent degenerate and near-degenerate systems," *Phys. Rev. A* **68**, 043818 (2003).
21. D. V. Brazhnikov, A. V. Taichenachev, A. M. Tumaikin, V. I. Yudin, S. A. Zibrov, Y. O. Dudin, V. V. Vasilev, and V. L. Velichansky, "Features of magneto-optical resonances in an elliptically polarized traveling light wave," *JETP Lett.* **83**, 64 (2006).
22. A. Lezama, S. Barreiro, and A. M. Akulshin, "Electromagnetically induced absorption," *Phys. Rev. A* **59**, 4732 (1999).
23. A. Javan, O. Kocharovskaya, H. Lee, and M. O. Scully, "Narrowing of electromagnetically induced transparency resonance in a Doppler-broadened medium," *Phys. Rev. A* **66**, 013805 (2002).
24. G. Wasik, W. Gawlik, J. Zachorowski, and W. Zawadzki, "Laser frequency stabilization by Doppler-free magnetic dichroism," *Appl. Phys. B* **75**, 613 (2002).
25. M. L. Haris, C. S. Adams, S. I. Cornish, L. C. McLeud, E. Tarleton, and I. G. Hughes, "Polarization spectroscopy in rubidium and cesium," *Phys. Rev. A* **73**, 062509 (2006).
26. C. Goren, A. D. Wilson-Gordon, M. Rosenbluh, and H. Friedmann, "Electromagnetically induced absorption due to transfer of coherence and to transfer of population," *Phys. Rev. A* **67**, 033807 (2003).
27. J. Alnis and M. Auzinsh, "Reverse dark resonance in Rb excited by a diode laser," *J. Phys. B: At. Mol. Opt. Phys.* **34**, 3889 (2001).
28. F. Renzoni and E. Arimondo, "Population-loss-induced narrowing of dark resonances," *Phys. Rev. A* **58**, 4717 (1998).
29. C. Goren, A. D. Wilson-Gordon, M. Rosenbluh, and H. Friedmann, "Atomic four-level N systems," *Phys. Rev. A* **69**, 053818 (2004).

1. Introduction

Electromagnetically induced absorption (EIA) is a phenomenon of increased absorption of radiation in atomic vapor resulting from the atomic coherence [1]. EIA is complementary effect to more thoroughly studied electromagnetically induced transparency (EIT). While EIT is related to a coherent population trapping (CPT) developed in a three-level Λ system [2], EIA is associated with low-frequency Zeeman coherences in a near-degenerate two-level system. EIA is observed in transitions when CPT can not be developed, that is when degeneracy in upper hyperfine level F_e is higher than in a ground hyperfine level F_g , where $F_{g,e}$ are total angular momentum of the ground and excited state, respectively [2, 3]. When external magnetic field is present and is taken as the quantization axis, EIA is explained by the spontaneous transfer of coherence induced between excited Zeeman sublevels, to the ground sublevels [4]. With quantization axis defined by the light polarization vector, EIA can be explained by the transfer of population [5, 6]. Investigations of EIA, like investigations of EIT are important because of the role of low-frequency Zeeman coherences in laser spectroscopy and quantum optics. Coherences between Zeeman sublevels play major role in sub-Doppler and sub-recoil laser cooling mechanisms [7, 8].

In atomic vapor with EIA increased laser absorption is accompanied by a steep anomalous dispersion and negative group velocity. Light storage and retrieval, demonstrated in media with

EIT [9], was also shown in gas vapor with EIA [10]. Yet there are much less studies of EIA compared to studies of EIT. EIA resonances were investigated in so-called Hanle configuration. Although Hanle effect was observed in fluorescence light where directions of exciting light and magnetic field were crossed [11] it is possible to explain it for arbitrary experimental geometry by density matrix approach. In the Hanle configuration of our experiment sub Doppler resonances are observed when external magnetic field B_z is scanned near zero value, due to the alignment of atoms induced by the laser at $B_z = 0$ and destroyed at $B_z > 0$. More specifically for our configuration, a single optical field, parallel to the external magnetic field is used and coherent effects are induced by its two counter-rotating circular polarization components. Theoretically Hanle effects were analyzed on a closed $F_g \rightarrow F_e = F_g + 1$ transition, by calculating a steady-state population of excited states at different laser intensities [5] and light polarization [12]. Previous experiments in Hanle configuration and on closed transitions show bright resonances due to EIA by measuring fluorescence emitted from vapor cells [12, 13, 14, 15, 16]. Studies of EIA resonances were also done with bi-chromatic field, when typically one measures transmission of a weak probe laser, as a function of its detuning in the presence of a strong pump laser (probe-pump studies) [1, 6, 17, 18, 19].

Vanishing and sign reversal of EIA, i.e., appearance of transmission peak at two photon resonance, was observed when laser light changes from linear to circular [14]), and when coherence of the excited state is significantly destroyed by collisions with the buffer gas [6]. Effect of laser intensity on Hanle EIA amplitude was predicted theoretically by Renzoni et al. [5]. Theoretical studies of probe laser EIA show that the EIA also vanishes at very high pump laser intensities. Such is the work by Taichenachev et al.[4], where, using a four-state N -scheme approximation, the probe EIA diminishes at high pump laser intensity. In very detailed study of open and closed $F_g = 1 \rightarrow F_e = 2$ transition for the D1 line of ^{87}Rb Goren et al., [20] have shown that for the same linear polarization of probe and pump lasers, probe EIA can switch to absorption dip only if Doppler broadening is not taken into account. Effect of Doppler broadening on EIA at various laser ellipticity was recently studied and it was shown that maximum of the EIA amplitude at the laser ellipticity different from zero can be explained only if Doppler effect is taken into account [21]. Experimental probe-pump studies of EIA have shown that a probe transmission keeps its EIA shape at high pump laser intensity [1, 22]. Using orthogonally polarized probe and pump lasers, Kim et al.[18] demonstrated the switch from EIA to a transmission peak at pump laser intensity of 150 mW/cm^2 .

In this work we have made experimental and theoretical investigation of the Hanle EIA dependence on the laser intensity for the laser tuned to $F_g = 3 \rightarrow F_e = 4$ transition in ^{85}Rb and $F_g = 2 \rightarrow F_e = 3$ in ^{87}Rb . We covered a wide range of laser intensities, below and above the saturation level. Our theoretical analyzes was done for the full atomic system of 16 Zeeman sublevels and for laser intensities used in the experiment. We also investigate, theoretically, effect of small stray laboratory magnetic field of a few mG on the shape of Hanle absorption spectra and on EIA amplitudes and widths. Amplitudes and widths of EIT as a function of laser intensity was thoroughly studied in homogeneously and inhomogeneously broadened medium [23]. There are not such studies of EIA. Previous data on EIA widths were observed in probe-pump studies, for the laser intensities $\leq 1 \text{ mW/cm}^2$ [1]. To our knowledge this work is the first detailed study of behavior of Hanle EIA amplitude and linewidth at broad range of laser intensities.

2. Experiment

The experimental set-up is shown in Fig. 1. Depending of the Rb cell we have used, the extended cavity diode laser (DL) is locked to either $F_g = 3 \rightarrow F_e = 4$ of ^{85}Rb or $F_g = 2 \rightarrow F_e = 3$ of ^{87}Rb hyperfine transitions of the D2 line using Doppler free dichroic atomic vapor laser lock

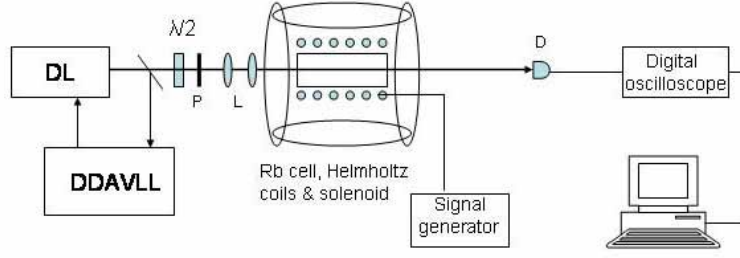


Fig. 1. Experimental set-up. DL - diode laser, L - collimating lenses, D - detector.

technique (DDAVLL) [24]. The plane of laser polarization was determined by linear polarizer (P), while the laser power was set by rotating half-wave plate ($\lambda/2$) in front of the polarizer. Results for the $F_g = 3 \rightarrow F_e = 4$ transition were obtained in 8 cm long Rb cell, while results for the $F_g = 2 \rightarrow F_e = 3$ transition were obtained in 1 cm long Rb cell (with enriched ^{87}Rb isotope). The cell was at room temperature. The cell is placed into the center of a large three pairs Helmholtz coils. Around the cell is a coaxial solenoid which provides the magnetic field B_z , parallel with the laser beam and the gas cell axis and is used to scan the magnetic field in the ± 1 G range. Before entering the cell the laser light is collimated by a pair of lenses (L) to a beam waist between 1 and 15 mm. Laser intensity is obtained from measured laser power and a beam profile at the sample. The input laser intensity was between 0.05 mW/cm^2 and 120 mW/cm^2 . Figure 2 shows absorption curves for two Rb cells. Normalized transmission, I_{out}/I_{in} , is between 35 – 60% and 60 – 75% for closed transitions in ^{85}Rb and ^{87}Rb , respectively. For values of laser intensities in the following discussions and figures we will state mean values of laser intensities in the cell, assuming its exponential decay in the cell.

3. Theory

In this section we present the model used to calculate transmission of a laser beam, resonant to the closed $F_g = 3 \rightarrow F_e = 4$ transition of ^{85}Rb . Optical Bloch equations were solved for density matrix elements $\rho_{i,j}$ for the atomic system of magnetic sublevels of both the ground $F_g = 3$ and of the excited $F_e = 4$ states. Zeeman sublevels are coupled by the linearly polarized laser field propagating in a direction of the external magnetic field. The model includes spontaneous transfer of low-frequency coherence of the excited sublevels to the ground states [4]. The optical Bloch equations, assuming pure radiative relaxation and the closed system, have the form

$$\begin{aligned} \dot{\rho}_{e_i e_j} &= \left[-\frac{2}{9} \Gamma_L |\mathcal{G}_1|^2 + i(\omega_{e_j} - \omega_{e_i}) \right] \rho_{e_i e_j} - \\ &\quad - \mathcal{G}_2 i \sum_{l=-3}^3 [\tilde{\rho}_{e_i g_l} (\mu_{g_l, e_j, -1} - \mu_{g_l, e_j, 1}) - \tilde{\rho}_{g_l e_j} (\mu_{e_i, g_l, -1} - \mu_{e_i, g_l, 1})] - \gamma \rho_{e_i e_j} \\ \dot{\tilde{\rho}}_{e_i g_j} &= \left[-\frac{\Gamma_L}{9} |\mathcal{G}_1|^2 + i(\omega_{(1)} + \omega_{g_j} - \omega_{e_i}) \right] \tilde{\rho}_{e_i g_j} - \\ &\quad - \mathcal{G}_2 i \left\{ \sum_{l=-4}^4 [\rho_{e_i e_l} (\mu_{e_l, g_j, -1} - \mu_{e_l, g_j, 1})] - \sum_{l=-3}^3 [\rho_{g_l g_j} (\mu_{e_i, g_l, -1} - \mu_{e_i, g_l, 1})] \right\} - \gamma \tilde{\rho}_{e_i g_j} \end{aligned}$$

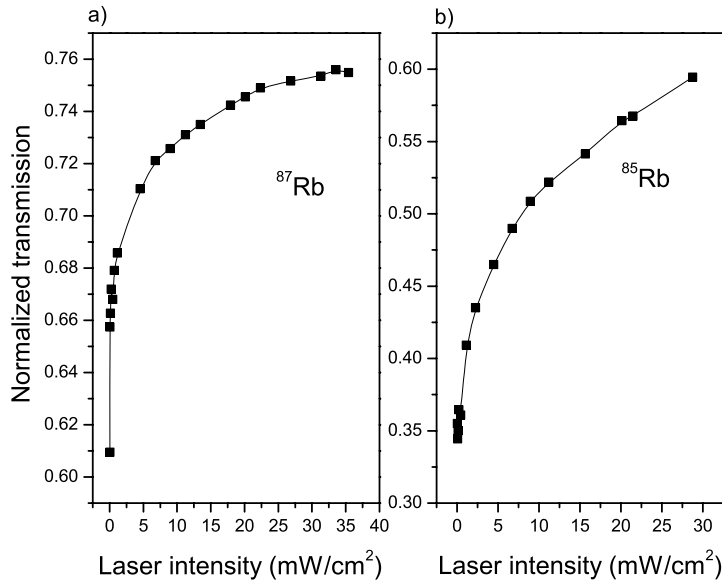


Fig. 2. Ratio of transmitted and input laser intensities as a function of the input laser beam intensity for: a) vacuum ^{87}Rb cell of 1 cm length (the laser is locked to the $F_g = 2 \rightarrow F_e = 3$) and b) vacuum Rb cell of 8 cm length (the laser is locked to the $F_g = 3 \rightarrow F_e = 4$), at room temperature at $B = 0$. Solid lines are drawn to guide the eye.

$$\begin{aligned} \dot{\rho}_{g_i g_j} = & \left[2(b + (1-b)\delta_{ij}) \sum_{q=-1}^1 \mu_{e_{i+q}, g_i, q} \mu_{e_{j+q}, g_j, q}^* \rho_{e_{i+q} e_{j+q}} \Gamma_L + i(\omega_{g_j} - \omega_{g_i}) \rho_{g_i g_j} \right] - \\ & - \mathcal{G}_2 i \sum_{l=-4}^4 [\tilde{\rho}_{g_i e_l} (\mu_{e_l, g_j, -1} - \mu_{e_l, g_j, 1}) - \tilde{\rho}_{e_l g_j} (\mu_{g_i, e_l, -1} - \mu_{g_i, e_l, 1})] - \\ & - \gamma \left(\rho_{g_i g_j} - \frac{1}{7} \delta_{ij} \right) \end{aligned} \quad (1)$$

where e and g refer to the ground and the excited state hyperfine levels, respectively. The diagonal elements of $\rho_{e_i e_j}$ ($\rho_{g_i g_j}$) are populations of e_j (g_i) sublevels, and off-diagonal elements are Zeeman coherences between $e_i e_j$ ($g_i g_j$) sublevels. Terms $\rho_{e_i g_j}$ represent optical coherences between e_i and g_j sublevels. Fast oscillations at laser frequency $\omega_{(1)}$ in Eq.1 were eliminated by the substitution

$$\rho_{e_i g_j} = \tilde{\rho}_{e_i g_j} e^{-i\omega_{(1)} t}. \quad (2)$$

The matrix elements of the electric dipole moments in Eq. 1 were calculated from

$$\mu_{e_{m_e}, g_{m_g}, q} = \mathcal{G}_1 (-1)^{-m_e} \begin{pmatrix} 3 & 1 & 4 \\ m_g & q & -m_e \end{pmatrix}. \quad (3)$$

where $q = 0, \pm 1$. Parameter \mathcal{G}_1 is proportional to the reduced matrix element of the dipole operator between the ground and the excited states.

$$\mathcal{G}_1 \sim \langle n_e L_e \| \mathbf{r} \| n_g L_g \rangle \quad (4)$$

Reduced matrix element is taken from [25]. In Eq. (1) $\omega_{e_i} \hbar$ and $\omega_{g_i} \hbar$ are energies of the atomic sublevels of the excited and ground levels, $\frac{2}{9} \Gamma_L |\mathcal{G}_1|^2 = \Gamma$, $\Gamma = 2\pi 5.89$ MHz is the decay rate of the excited state. $\mathcal{G}_2 = \frac{E_{(1)0}}{2\sqrt{2}\hbar}$ and $E_{(1)0}$ is the amplitude of the laser electric field. The laser electric field written in the rotation coordinate system with unit vectors $\mathbf{u}_{\pm 1}$ ($\mathbf{u}_{-1} = \frac{\mathbf{e}_x - i\mathbf{e}_y}{\sqrt{2}}$, $\mathbf{u}_{+1} = -\frac{\mathbf{e}_x + i\mathbf{e}_y}{\sqrt{2}}$) is

$$\mathbf{E}(\mathbf{r}_0, t) = \frac{\mathbf{u}_{-1} - \mathbf{u}_{+1}}{2\sqrt{2}} e^{-i\omega_{(1)}t} \cdot E_{(1)0} \quad (5)$$

Laser detuning is given by $\Delta = \Delta_S + \Delta_R$, where $\Delta_S = \omega_{(1)} + \omega_{g_0} - \omega_{e_0}$ (difference between laser frequency and D2 line) is a single photon detuning, and Δ_R is a Raman, two-photon detuning due to Zeeman splitting. Raman detuning is calculated from Zeeman splitting of ground and excited states using $\Delta_{g(e)} = 1.39962 g_{F_{g(e)}} \text{ MHz/Gauss}$, where $g_{F_{g(e)}}$ is the Lande g -factor for two hyperfine levels. For ^{85}Rb splittings of $F_e = 3$ and of $F_e = 4$ levels with magnetic field are 0.46 MHz/Gauss and 0.7 MHz/Gauss, respectively. The light Rabi frequency of the individual transition is

$$\Omega_{R_{g_k e_j}} = \mathcal{G}_2 \mu_{g_k e_j} \quad (6)$$

The first term in the expression for $\rho_{g_i g_j}$ in (1) corresponds to the transfer of population and of coherence from the excited to the ground level [4, 26]. The parameter $0 \leq b \leq 1$ is the amount of off-diagonal elements $\rho_{e_i e_j}$ transferred onto coherences in ground states $\rho_{g_i g_j}$. The theoretical results presented below are for $b = 1$. The ground state relaxation rates were taken into account by γ . In the vacuum Rb cell at room temperature γ is determined by the atom transit time through the laser beam. Under these assumption we have calculated γ from $\gamma = v_{mp}/r$, where $v_{mp} = \sqrt{2k_B T/M}$ is the most probable velocity of the atoms (equal ~ 240 m/s for Rb atoms at room temperature [27]) and r is the radius of the laser beam. In our theoretical treatment, the change in the laser beam intensity along the Rb cell (Fig. 2) and along the laser beam diameter (usually Gaussian profile) have not been taken into account. The effect of magnetic field transversal to B_z was included by the way of quantization axis along the total magnetic field.

The system of equations given in (1) was solved assuming a steady state of an atomic system. Such approximation is correct for cold atoms, like for laser cooled atomic gas, when the interaction time between the atoms and the laser are long enough so that a steady-state is reached. Our experimental results can be compared to the steady state solution of the Eq. (1) since the estimated atom transit time through the laser beam is longer than calculated time required for atoms to reach a steady state when suddenly illuminated by light tuned to a closed transition [28]. Light absorption is calculated from the sum of populations of all magnetic substates of the excited state, i.e., diagonal density matrix elements, $\sum \rho_{e_i e_i}$. Theoretical results shown below are in fact presented as a laser transmission, obtained after subtracting total absorption from unity. Note that measurements of total fluorescence is also a measure of the total light absorption, assuming the same decay rate for all sublevels. Calculations were performed for the same range of the laser intensities as in the experiment.

4. Discussion

4.1. Experimental results

Figure 3 shows experimental Hanle EIA for two laser intensities, 0.1 and 11 mW/cm², for transition $F_g = 2 \rightarrow F_e = 3$ in ^{87}Rb and for the laser beam diameter of 2.5 mm. For intensities above these, experimental results also show characteristic EIA shape, like curves in Fig. 3. These curves were obtained by averaging more than 500 samples on the storage oscilloscope.

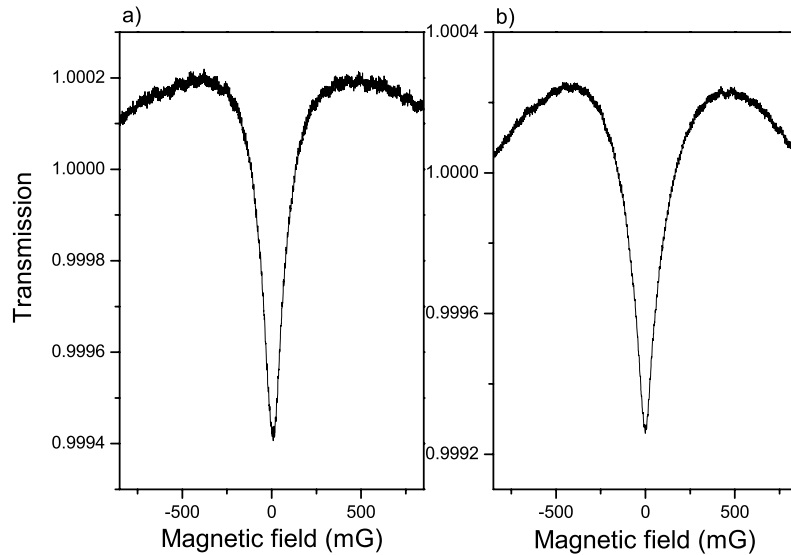


Fig. 3. Hanle EIA for (a) 0.1 mW/cm² and (b) 11 mW/cm² of the laser intensity. The laser is locked to the D2 $F_g = 2 \rightarrow F_e = 3$ transition in ⁸⁷Rb; beam diameter is 2.5 mm.

Experimental results for the Hanle EIA amplitude and width as a function of the laser intensity are given in Fig. 4 for the $F_g = 2 \rightarrow F_e = 3$ transition in ⁸⁷Rb, and in Fig. 5 for $F_g = 3 \rightarrow F_e = 4$ transition in ⁸⁵Rb. Solid lines in figures are to guide the eye. We evaluated amplitudes and widths at the interval of magnetic fields between -1 and 1 G. On these range there are no complex curves like these in Fig. 7(b) and only one peak is observed. Amplitude was evaluated like the difference between maximum of the curve and a minimum between 2 maxima. Width is a full width at half of the amplitude of the Hanle transmission curves. This method agrees with fitting the curves with double Lorentzian. Data points in these curves were also obtained after fitting transmission curves, like curves in Fig. 3 by double Lorentzian. One of Lorentzian represents a wider Hanle signal, much wider than our scanning range. Second Lorentzian represents EIA resonance which is of opposite sign than Hanle signal. Widths present domain of magnetic field in which Zeeman coherences are not yet destroyed. Note that data given in two figures were obtained using two Rb cells. For results in Fig. 4 we used 1 cm long cell with enriched 87 isotope. Both amplitude and width of the EIA have maximums. From results presented in Figs. 4 and 5 it follows that maximums for 85 and 87 isotopes appear at similar laser intensities after correction for different laser absorption (due to different absorption coefficients and different cell lengths, Fig. 2) are taken into account. Insert in Fig. 4(a) shows amplitude variations at lowest laser intensities. This interesting width narrowing of EIA at high laser intensity is in contrast to well established EIT behavior vs laser intensity. The errors for widths and amplitudes, given by error bars in Figs. 4 and 5 were estimated from experimental conditions and they are primarily due to presence of laboratory stray magnetic field, quality of polarizing optics, stability of laser intensity and frequency, and errors originating from fitting transmission curves. We like to note that we made few measurements at much higher intensities than those presented in Figs. 4 and 5. For the laser intensity of 100 mW/cm² (obtained when using 1 mm diameter laser beam), we also had similar results in a sense that

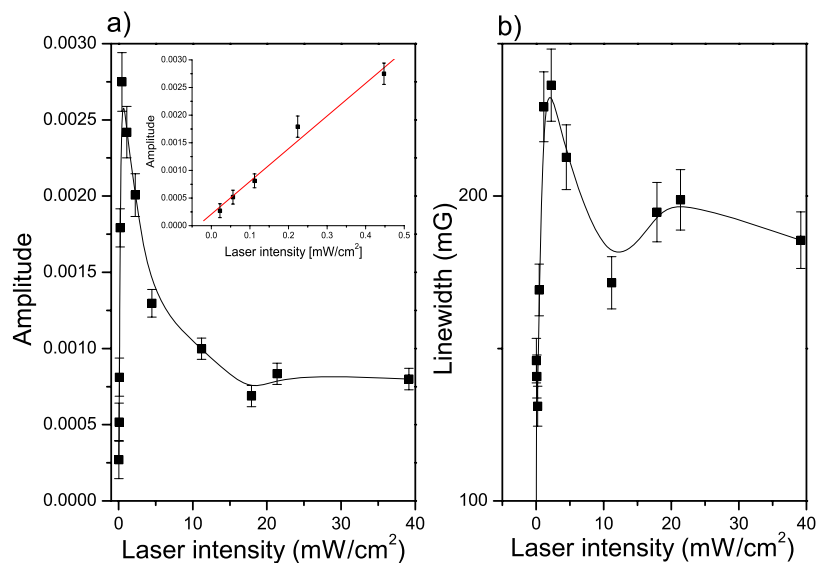


Fig. 4. (a) Amplitude of the Hanle EIA and (b) Full width at half maximum and as a function of the laser intensity for $F_g = 2 \rightarrow F_e = 3$ transition in ^{87}Rb . Points in the insert are experimental data for at lowest laser intensities and line is the linear fit.

transmission minimum at $B_z=0$ remains at steady value, and never changed sign.

Dependence of the EIA width on the inverse value of the laser beam diameter, for the laser intensity of 0.8 mW/cm^2 is shown in Fig. 6. Solid line is a linear fit with a coefficient $410 \pm 75 \text{ mG mm}$. Such dependence of the widths suggests that at these intensities inverse of atomic time of flight through the laser beam can be taken as coherence decay (like in our calculations). Dependence of Hanle EIA width is similar to the result observed in the atomic fluorescence in the pump-probe experiment [1].

4.2. Theoretical results

Numerical calculations for transmission of the laser were done for the atomic transition $F_g = 3 \rightarrow F_e = 4$ in ^{85}Rb . Detunings of the order of a few MHz simulate experimental transmission curves (Fig. 3) better than zero detuning. Results in Fig. 7 are for the laser detuning $\Delta_S = \pm 3 \text{ MHz}$. In Fig. 7(a) the laser intensity is 0.1 mW/cm^2 , and in Fig. 7(b) we present calculations for higher laser intensities, from 1 to 40 mW/cm^2 . Small EIA, still observed at 1 mW/cm^2 at the center of wide transmission gain disappears at 3 mW/cm^2 . Calculations of transmission of a probe laser in probe-pump studies show that probe EIA changes with a laser intensity and, similar to a Hanle EIA, switches to a transmission peak at high Rabi frequency [4, 29].

Residual magnetic fields at the location of the Rb cell also influence the shape, amplitude and width of EIA. Magnetic fields transversal to B_z field, measured at the center of large Helmholtz coils, are $< 5 \text{ mG}$. Such level of stray magnetic field should not change the amplitude or the width of the EIA, according to our calculations. Calculated EIA curve for transversal magnetic field of 20 mG (dashed line in 7(a)) shows very small difference from the curve at zero transversal magnetic field.

In a gas with Maxwell velocity distribution, total transmission is a superposition of trans-

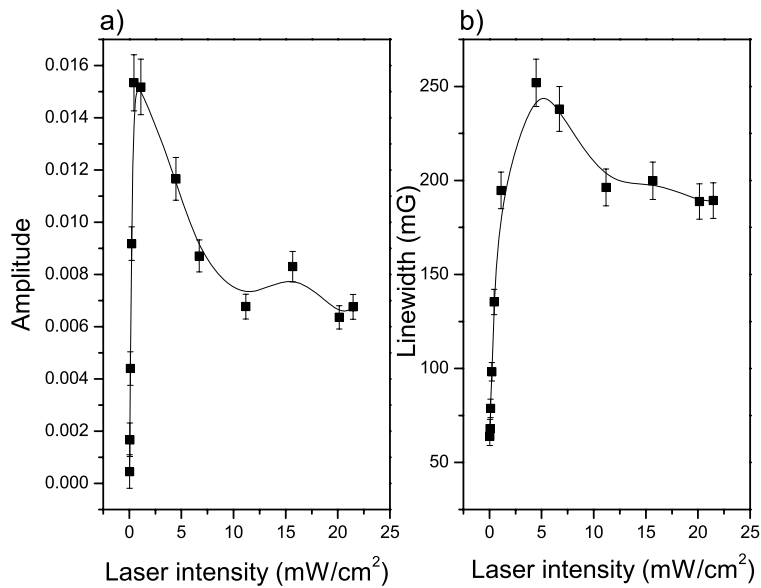


Fig. 5. (a) Amplitude of the Hanle EIA, (b) Full width at half maximum and as a function of the laser intensity for $F_g = 3 \rightarrow F_e = 4$ transition in ^{85}Rb .

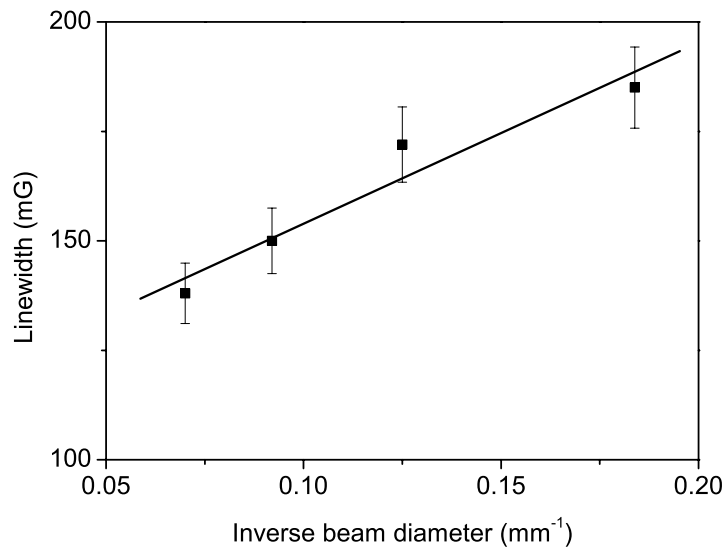


Fig. 6. Full width at a half maximum of the EIA as a function of inverse laser beam diameter. The solid line is linear fit through the data. The laser intensity is $0.8 \text{ mW}/\text{cm}^2$.

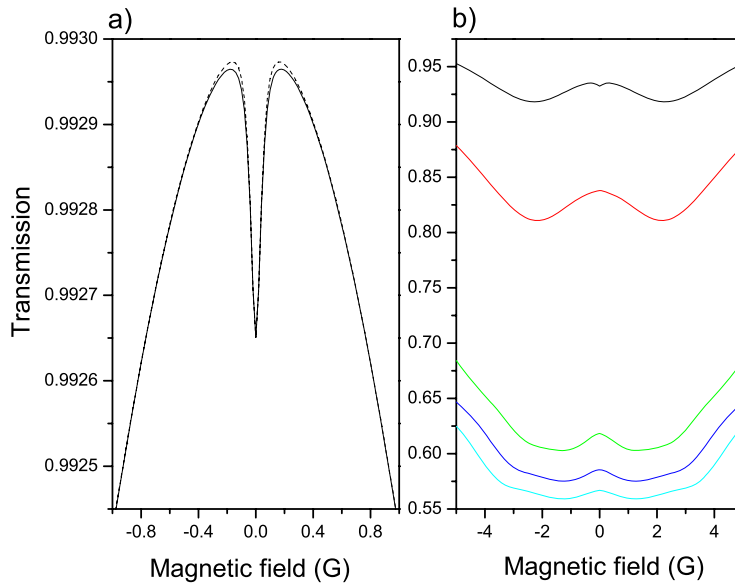


Fig. 7. Calculated transmission of linearly polarized input laser, detuned by $\Delta = 3$ MHz from the $F_g = 3 \rightarrow F_e = 4$ transition in ^{85}Rb , as a function of the magnetic field for laser intensity (a) 0.1 mW/cm^2 (transversal magnetic field zero (solid line) and 20 mG (dashed line)), and (b) $1, 3, 20, 30$ and 40 mW/cm^2 for curves from top to bottom, respectively. Please note different scales for magnetic fields in (a) and (b).

missions calculated for different velocities i.e., corresponding detunings Δ_S . Each of these calculated curves has certain weight. Maxwell-Boltzmann velocity distribution gives wide Doppler inhomogeneous broadening, but most of atoms have values of v_z (z -axis components of velocities, direction of laser light propagation) such that laser detuning due to Doppler effect is in the range of a few MHz. Theoretical results for the EIA amplitudes and widths, as a function of the laser intensity, are given in Fig. 8. Curves in Fig. 8 correspond to different laser detunings $\Delta_S \neq 0$. They show that intensities at which EIA amplitude has maximum and intensities at which EIA vanishes, strongly depend on the laser detuning. As laser detunings increase, they both move towards larger laser intensities. Moreover, at temperature $T = 300 \text{ K}$ even atomic velocities corresponding to detunings of several hundreds of MHz have a non-negligible weight. Theory indicates that at such large detunings, amplitude and width do not fall to zero at the highest experimental laser intensity or even higher. Very important conclusion then follows from theoretical results: we were not able to experimentally observe vanishing of EIA, because of Doppler broadening.

Behavior of EIT amplitude and width at low and high laser intensities were studied previously. Javan et al., [23] in their thorough analyzes gave analytical expressions for EIT widths as a function of the laser intensity. They found square-root dependence at low laser intensity (below saturation) and linear dependence at higher laser intensity. We have shown in this work that EIA amplitude and width behave quite differently with increasing laser intensity. These results can be understood from numerical results of the population, ρ_{g_i, g_i} , and of coherence, ρ_{g_i, g_j} of Zeeman sublevels of the ground state hyperfine level as a function of the laser intensity.

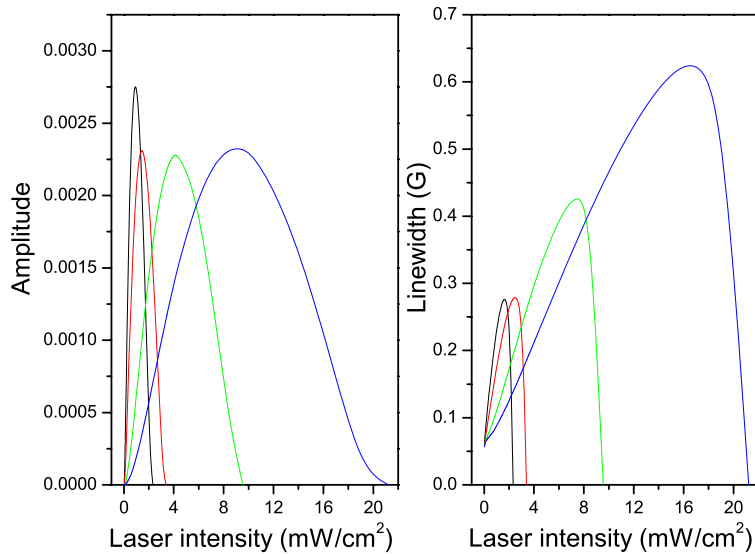


Fig. 8. Calculated (a) amplitude and (b) width of the EIA as a function of the laser intensity when input light is near-resonant to $F_g = 3 \rightarrow F_e = 4$ transition in ^{85}Rb . Maximum of both EIA amplitude and width shifts to higher laser intensities as the laser detuning takes values 3, 5, 10, 15 and 20 MHz.

ties. Figure 9 shows how the populations of each Zeeman level change with the laser intensity. When we choose quantization axis parallel to the external magnetic field B_z , the laser pumps the population in the ground state Zeeman sublevels $m_{F_g} = \pm 3$. This is not the result of a strong correlation among sublevels of the same hyperfine state, instead it is the result of saturation of the Zeeman sublevels of $F_e = 4$, via strong coupling between $m_{F_g} = 3$ and $m_{F_e} = 4$ sublevels. With increasing laser intensity, population of ground sublevels $m_{F_g} = \pm 3$ goes through a maximum and increasing laser detuning moves this maximum towards higher laser intensities. This can explain observed behavior of EIA amplitude.

5. Conclusion

In this paper we presented experimental and theoretical results for amplitudes and widths of the Hanle EIA, obtained with the laser resonant to close $F_g \rightarrow F_e = F_g + 1$ transitions in both ^{85}Rb and ^{87}Rb , as a function of the laser intensity. Amplitudes and widths were obtained from measured and calculated absorption resonances for the range of external magnetic field $B_z = \pm 1$ G. Effect of laboratory stray magnetic field on such resonances was evaluated theoretically and was found that measured residual, transversal (in respect to B_z) magnetic field below 5 mG does not influence the main result of the paper. Same results of EIA amplitude and width obtained with two Rb cells of very different lengths, also indicate that stray magnetic field was well compensated.

Both amplitude and width of the EIA, as a function of laser intensities, have maximums. Therefore, EIA behaves differently from well known behavior of EIT. Behavior of the theoretical EIA amplitudes and widths depends on the laser detuning - detuning influences intensity corresponding to maximums of amplitude and width. Beyond the maximum, theoretical EIA

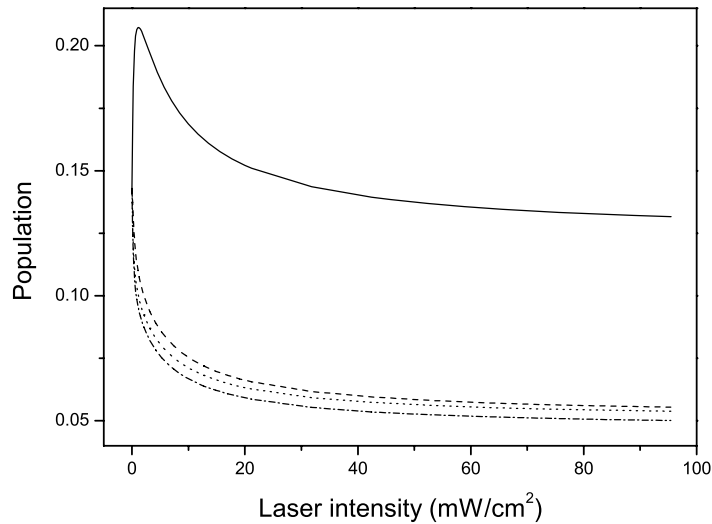


Fig. 9. Calculated population of Zeeman sublevels of $F_g = 3$ in ^{85}Rb as a function of the laser intensity; $m_F = \pm 3$ (solid line), $m_F = \pm 2$ (dashed line), $m_F = \pm 1$ (dotted line), $m_F = 0$ (dashed-dotted line).

amplitude goes to zero and then switches sign to a broad transmission gain. Instead, experimental EIA amplitude and width saturates at the value different from zero. Theoretical results of the EIA amplitude and widths at different laser detunings suggest that the reason for discrepancies between theory and experiment is Doppler effect present in the experiment. Appearance of the maximum of the EIA amplitude, at particular laser intensity, can be understood from similar behavior of the loss of population of the ground state Zeeman sublevels, most coupled by the laser light.

Acknowledgments

This work was supported by the Ministry of science and environmental protection of the Republic of Serbia, under grant number 141003.